

Proceeding Paper

Hydrogel-Coated Nanonet-Based Field-Effect Transistors for SARS-CoV-2 Spike Protein Detection in High Ionic Strength Samples †

Alexandra Parichenko ¹, Wonyeong Choi ², Seonghwan Shin ², Marlena Stadtmüller ³, Teuku Fawzul Akbar ⁴, Carsten Werner ⁴, Jeong-Soo Lee ^{2,*}, Bergoi Ibarlucea ^{1,*} and Gianarelio Cuniberti ^{1,*}

¹ Institute for Materials Science and Max Bergmann Center for Biomaterials, Dresden University of Technology, 01062 Dresden, Germany; alexandra.parichenko@tu-dresden.de

² Department of Electrical Engineering, Pohang University of Science and Technology (POSTECH), Pohang 37673, Republic of Korea; pathfinder@postech.ac.kr (W.C.); ssh3290a@postech.ac.kr (S.S.)

³ Universitätsklinikum Carl Gustav Carus Dresden, 01307 Dresden, Germany; marlena.stadtmueller@uniklinikum-dresden.de

⁴ Max Bergmann Center for Biomaterials, Leibniz Institute of Polymer Research Dresden, 01069 Dresden, Germany; akbar@ipfdd.de (T.F.A.); werner@ipfdd.de (C.W.)

* Correspondence: ljs6951@postech.ac.kr (J.-S.L.); bergoi.ibarlucea@tu-dresden.de (B.I.); gianarelio.cuniberti@tu-dresden.de (G.C.)

† Presented at the 3rd International Electronic Conference on Biosensors, 8–21 May 2023; Available online: <https://iecb2023.sciforum.net/>.

Abstract: The SARS-CoV-2 pandemic has triggered many studies worldwide in the area of biosensors, leading to innovative approaches for the quantitative assessment of COVID-19. A nanostructured field-effect transistor (FET) is one type of device shown to be ultrasensitive for virus determination. FETs can be used as transducers to analyze changes in electrical current caused by the bonding of viral molecules to the surface of the semiconducting nanomaterial layer of the FETs. Although nano-transistors require simple setups amenable to be miniaturized for point-of-care diagnostic of COVID-19, this type of sensor usually has limited sensitivity in biological fluids. The reason behind this is the shortened screening length in the presence of high ionic strength solutions. In the frame of this study, we propose a methodology consisting of the FET surface modification with a hydrogel based on the star-shaped polyethylene glycol (starPEG), which hosts specific antibodies against SARS-CoV-2 spike protein in its porous structure. The deposition of the hydrogel increases the effective Debye length, preserving the biosensor's sensitivity. We demonstrate the capability of silicon nanonet-based FETs to detect viral antigens and cultured viral particles in phosphate-buffered saline (PBS) as well as in human-purified saliva. Finally, we discriminated between positive and negative patients' nasopharyngeal swab samples.

Keywords: COVID-9 diagnostics; SARS-CoV-2 detection; hydrogel biosensor; field-effect transistor; Debye screening length; starPEG



Citation: Parichenko, A.; Choi, W.; Shin, S.; Stadtmüller, M.; Akbar, T.F.; Werner, C.; Lee, J.-S.; Ibarlucea, B.; Cuniberti, G. Hydrogel-Coated Nanonet-Based Field-Effect Transistors for SARS-CoV-2 Spike Protein Detection in High Ionic Strength Samples. *Eng. Proc.* **2023**, *35*, 11. <https://doi.org/10.3390/IECB2023-14566>

Academic Editor: Danila Moscone

Published: 8 May 2023



Copyright: © 2023 by the authors. Licensee MDPI, Basel, Switzerland. This article is an open access article distributed under the terms and conditions of the Creative Commons Attribution (CC BY) license (<https://creativecommons.org/licenses/by/4.0/>).

1. Introduction

As an alternative to the standard techniques of Covid-19 [1] diagnostics, novel miniaturized electronic devices have been introduced for rapid detection even in asymptomatic carriers of the virus or in individuals with low viral load. Miniaturization of electrochemical techniques was demonstrated by several studies using commercially available screen-printed electrodes and small-footprinted potentiostats, where authors performed the measurements with either immunosandwich assays with labeled secondary antibodies [2] or redox mediators [3] to provide the electrical signal. Alternative electronic biosensing devices are field-effect transistors (FETs). They sense even minor alterations in the electrical

signal caused by simple biorecognition events without the need for redox mediators or receptors labeled with electroactive tags.

A number of FET-based biosensors have already been reported for the detection of SARS-CoV-2 antigens [4,5]. FETs based on silicon nanowires are known to have excellent sensitivity [6,7]. However, they are also known for their severe limitation based on the Debye length screening distance when immersed in high ionic strength samples [8]. As a result, the conductivity changes caused by the binding of target pathogens to the bioreceptors may not be detected by the biosensor. A promising solution to this problem was found via surface chemistry by the co-deposition of the dielectric polyethylene glycol (PEG) on the surface of the FET [9]. However, two-dimensional surface modification approaches still suffer from certain disadvantages compared to three-dimensional ones, such as limited interaction kinetics between the surface and the sample and possible instability of the bioreceptors. The incorporation of PEG and antibodies as a three-dimensional fluid-like environment in the form of hydrogels introduces a new way of FET-based biosensing where the effective Debye length is increased, offering an increased degree of receptor-analyte interaction and a higher degree of surface protection from undesired non-specific interactions.

In this contribution, we demonstrate antibody–antigen binding transduction in high ionic strength using PEG-based hydrogels as host environments for the receptors and nanomaterial-based FETs as transducers. Specifically, we used the star-shaped PEG hydrogel where antibodies against the spike protein of the novel coronavirus (SARS-CoV-2) are hosted. Silicon nanonet-based FETs were used to perform spike protein detection in spiked buffer, spiked saliva, cultured viral solutions, and real samples from nasopharyngeal swabs.

2. Results and Discussion

The used FETs consist of microfabricated electrodes with a silicon nanonet with lateral distances of 100 nm at the interconnects (Figure 1a) covered with the starPEG-based hydrogel. The hydrogel deposition resulted in the formation of a receptor molecule hosting platform homogeneously distributed on top of the FETs gate electrode and the regions with the nanonet. The homogeneous shaping of the hydrogel layer with a thickness of ca. 35 μm (Figure 1b) was achieved due to the pressure from the applied glass slide.

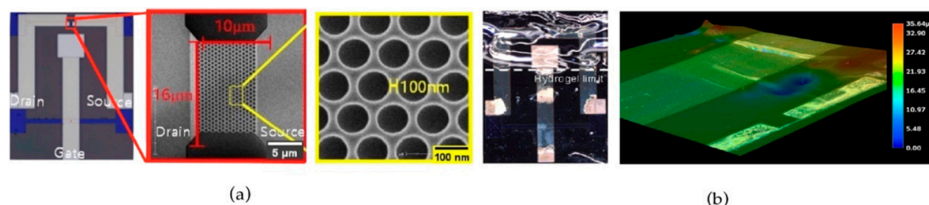


Figure 1. FET characterization: (a) optical microscopy of unmodified FETs and SEM magnification of the sensing area, and (b) hydrogel-modified FET and its 3D profile.

During the FETs transfer characteristics recording the drain-source current I_{ds} was monitored, while the gate voltage V_{g} of the devices was swept with applied constant source-to-drain potential V_{ds} equal to 0.1 V. After each incubation of the samples on the biosensing platform with increasing concentrations of spike protein receptor binding domain (RBD) (from 5 pg mL^{-1} to 50 ng mL^{-1}) in PBS (Figure 2a), the signal was measured in pure PBS. Significant concentration dependency of the transfer curve was observed (Figure 2a,b). The FET-based biosensor covered with hydrogel showed a sensitivity of 30 $\text{mV} \pm 5.7 \text{ mV}$ to a ten-fold increase of spike protein concentration in PBS. The voltage shift direction is in agreement with the theoretical isoelectric point of 3.9 and negative net charge at pH 7.4 ($z = -1.483$) for the amino acid sequence of the RBD (region 480–499: cngvegfncyfplqsygfpq). In comparison, the performance in a diluted buffer demonstrated similar sensitivity to the antigens concentration changes (31 $\text{mV} \pm 3.5 \text{ mV}$). These results suggest that the hydrogel layer on top of the FETs preserves the sensitivity of the device

in high ionic strength solutions. Non-specific interactions of the sensor were discarded by exposing the hydrogel to human IgG (Figure 2b).

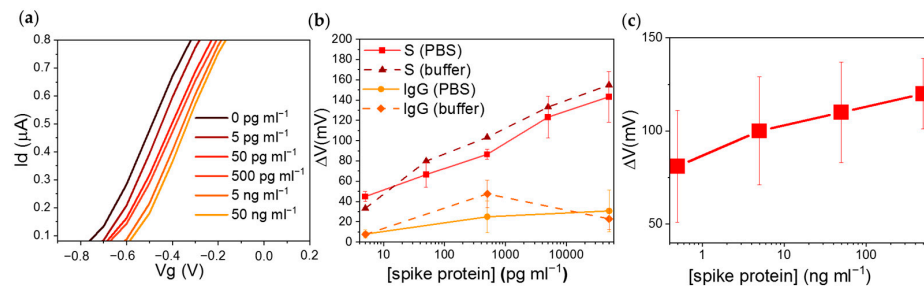


Figure 2. Electrical measurements results: (a) Biosensor response on different concentrations of SARS-CoV-2 RBD dissolved in PBS. (b) Dependency of the gate voltage shift on antigens concentration in PBS and diluted phosphate buffer (5 mM), with error bars indicating the standard deviation of three different sensors. (c) The gate voltage shift dependency (with error bars as the standard deviation of three sensor measurements) on corresponding antigen concentration dissolved in purified saliva.

Purified saliva spiked with RBD was used to assess the capability of the biosensor to detect the presence of COVID-19 pathogens in complex biological fluids. Although recorded I–V curves demonstrated clear dependence on the antigen concentration (Figure 2c), the achieved sensitivity was smaller in comparison to those obtained in PBS (20 mV \pm 9 mV to ten-fold increase of RBD concentration). Our assumption is that the reason for this is the higher viscosity of human saliva in comparison to PBS, which could lead to a reduced diffusion of the molecules and, therefore, a diminished interaction between the target and bioreceptors.

Before measuring patients’ samples, we analyzed samples of cultured viruses to confirm that spike protein was detectable after inactivation. Incubation of the hydrogel layer with heat-deactivated samples (80 °C for 1 h [10]) led to consistent signals with clear dependence of the FETs gate voltage shift on the virus concentration (Figure 3a). Further measurements with heat-inactivated samples of COVID-19-positive (CT value 15.8) and negative patients proved the capability of the device to identify the presence of the virus in a realistic clinical scenario (Figure 3b). The I–V curve recorded after incubation with the negative sample overlapped with the baseline originated from a measurement with only PBS, while the incubation with COVID-19 positive sample resulted in a significant shift of the signal (105 mV). Additionally, the transfer characteristics of the biosensor were also recorded for different dilutions of heat-inactivated viral samples from nasopharyngeal swabs (Figure 3c). All three devices used for the measurements demonstrated a clear dependence on the FETs gate voltage shift on the concentration of the inactivated viral samples.

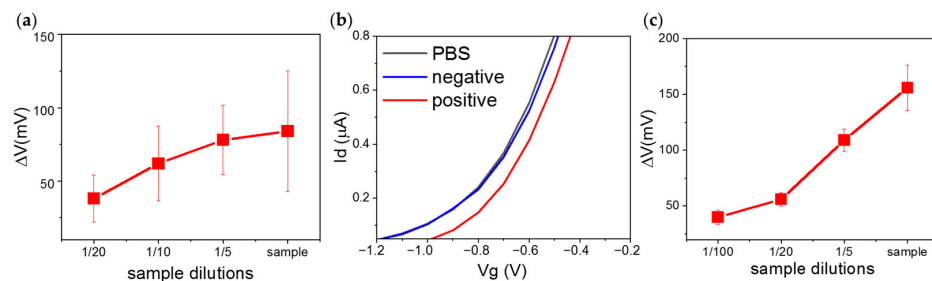


Figure 3. Measurements with viral samples: (a) Biosensor response on different dilutions of heat-inactivated cultured viral particles suspended in PBS (with error bars as the standard deviation of three sensor measurements). (b) FETs transfer characteristics recorded after incubation of the biosensor with COVID-19-negative (blue) and COVID-19-positive (red) heat-inactivated nasopharyngeal swabs from patients. (c) Biosensor response on different dilutions of heat-inactivated viral samples from nasopharyngeal swabs suspended in PBS.

3. Conclusions

In the frame of this study, we demonstrated the capability to use FETs coated with the starPEG-heparin hydrogel-containing antibodies for direct SARS-CoV-2 detection in high ionic strength solutions. This was proven by consecutive incubation of the biosensing hydrogel platform with different concentrations of spike protein RBDs dissolved in PBS solution, and the observation of the I–V curves shift to more positive values after each incubation-washing cycle. Thus, we confirmed the dependency of the signal on the target protein concentration in the analyzed liquid samples. Additionally, it was possible to sense the change of the RBD concentration on femtomolar levels in diluted and undiluted buffer, overcoming the Debye length limitation. The biosensor was able to perform the detection in femtomolar levels of the analyte in both conditions, high and low ionic strength, demonstrating the ultrasensitivity required for early diagnostics. Successful results by spiking human purified saliva showed the potential use of such fluid as a non-invasive source, offering an alternative to the uncomfortable nasopharyngeal swab. Finally, real samples in the form of cultured viruses could be measured, and nasopharyngeal swabs from healthy and sick patients could be discriminated. However, to achieve a quantitative result with saliva and real samples with high viral load, sample dilution would be beneficial due to the sensor signal saturation.

All in all, we showed the suitability of pegylated hydrogels as a new method to overcome the Debye length problem in samples with high ionic strength, providing the advantages of such hydrogels to protect the sensor surface from non-specific adsorption and preserve the activity of antibodies. Further improvement may be necessary to avoid saturation of the device after incubation with highly concentrated samples. The opportunity to quantitatively measure the virus concentration by this biosensor may be helpful for obtaining an overview of the infection and disease situation. In addition, the biosensor can be used as a rapid early test to avoid overloading medical facilities, additionally, in view of future epidemics or pandemics, by adjusting the hydrogel composition according to the needs of other receptors and target biomarkers.

4. Methods

4.1. Silicon Nanonet-Based Field-Effect Transistor Fabrication

KrF photolithography and inductively coupled plasma reactive ion etching was used as a highly reproducible method to define the active region on silicon-on-insulator wafers with a 100 nm top Si layer (p-type, 10 Ω -cm, (100)) and a 400 nm buried oxide layer. The source and drain regions were formed by arsenic ion implantation with a dose concentration of $5 \times 10^{15} \text{ cm}^{-2}$. A 5 nm oxide was grown as a gate insulator by rapid thermal annealing at 1000 °C for 20 s. The contact pads, source/drain transmission lines, and gate electrodes were formed using an I-line stepper and a lift-off process. Finally, a SU-8 passivation layer was formed on the entire surface except for the contact pads, channel, and reference electrode regions.

4.2. Hydrogel Preparation and Deposition

StarPEG-heparin hydrogel was prepared via Michael addition reaction, where PEG-thiol reacted with heparin maleimide 6 in the presence of the antibodies against SARS-CoV-2 RBD epitope (480–499). Details can be found in ref. [11]. The final mixture was drop cast on top of the FETs for in situ gelation. A glass slide was put on top for 60 min in order to achieve a homogeneous and flat surface. Finally, the glass slide was removed, and the gel was hydrated using PBS.

4.3. Optical Microscopy and Thickness Estimation

Optical microscopy of the hydrogel layer was done using a digital microscope (VHX-7000, Keyence Deutschland, Neu-Isenburg, Germany). The layer of star-PEG-heparin was visualized on top of the FET chip surface. The scanning mode of the microscope provided a 3D profile to estimate the thickness of the hydrogel after the deposition procedure described above.

4.4. Virus Culture and Deactivation

Virus isolates were obtained from nasopharyngeal swabs of anonymous patients. The swab sample was filtered through a 0.2 μm filter and then added to Vero E6 cells cultured in DMEM GlutaMAX supplemented with 10% fetal bovine serum, 1% non-essential amino acids, and 1% penicillin/streptomycin. The virus was harvested upon the destruction of the cell layer. The supernatant was cleared by centrifugation to remove cell debris. Passage two of any isolate was used for experiments. Virus stocks were inactivated by heating for 1 h at 80 °C.

4.5. Electrical Measurements

All I–V curves with FETs were obtained using a source measure unit (2604B, Keithley Instruments, Germering, Germany) in a probe station with micropositioners for electrical connection. For the biosensing response, the hydrogel-FET was incubated for 15 min with 4 μL of the target solution. Every incubation step was followed by washing in pure PBS in order to remove unbound antigens and other possible molecules or cell debris. Measurements were taken after each incubation-washing cycle using either a drop of PBS (4 μL) as a high ionic strength solution or a drop of the same volume of 5 mM sodium phosphate buffer as a low ionic strength solution.

Author Contributions: A.P. performed the biosensing experiments, analyzed the results, prepared the figures, and wrote the manuscript with feedback and revision from all authors. W.C. and S.S. fabricated the field-effect transistors coordinated and supervised by J.-S.L. M.S. prepared the viral samples including their inactivation. T.F.A. prepared the hydrogel supervised by C.W. B.I. conceived and supervised the overall work with feedback from G.C. G.C. acquired the funding. All authors have read and agreed to the published version of the manuscript.

Funding: This research was funded by the Sächsische AufbauBank, grant number 100525920.

Institutional Review Board Statement: All clinical samples were retrieved from biobanks. The study was conducted according to the guidelines of the Declaration of Helsinki and all protocols and registries have been approved by the Ethics Committee of the TU Dresden. All participants have provided signed written informed consents.

Informed Consent Statement: Informed consent was obtained from all subjects involved in the study.

Data Availability Statement: The data is available from the corresponding authors upon reasonable request.

Acknowledgments: This work was funded by the Sächsische AufbauBank project 100525920.

Conflicts of Interest: The authors declare no conflict of interest.

References

1. Rasmi, Y.; Li, X.; Khan, J.; Ozer, T.; Choi, J.R. Emerging point-of-care biosensors for rapid diagnosis of COVID-19: Current progress, challenges, and future prospects. *Anal. Bioanal. Chem.* **2021**, *413*, 4137–4159. [[CrossRef](#)]
2. Vásquez, V.; Navas, M.-C.; Jaimes, J.A.; Orozco, J. SARS-CoV-2 electrochemical immunosensor based on the spike-ACE2 complex. *Anal. Chim. Acta* **2022**, *1205*, 339718. [[CrossRef](#)]
3. Eissa, S.; Zourob, M. Development of a Low-Cost Cotton-Tipped Electrochemical Immunosensor for the Detection of SARS-CoV-2. *Anal. Chem.* **2021**, *93*, 1826–1833. [[CrossRef](#)]
4. Zamzami, M.A.; Rabbani, G.; Ahmad, A.; Basalah, A.A.; Al-Sabban, W.H.; Nate Ahn, S.; Choudhry, H. Carbon nanotube field-effect transistor (CNT-FET)-based biosensor for rapid detection of SARS-CoV-2 (COVID-19) surface spike protein S1. *Bioelectrochemistry* **2022**, *143*, 107982. [[CrossRef](#)]
5. Seo, G.; Lee, G.; Kim, M.J.; Baek, S.-H.; Choi, M.; Ku, K.B.; Lee, C.-S.; Jun, S.; Park, D.; Kim, H.G.; et al. Rapid Detection of COVID-19 Causative Virus (SARS-CoV-2) in Human Nasopharyngeal Swab Specimens Using Field-Effect Transistor-Based Biosensor. *ACS Nano* **2020**, *14*, 5135–5142. [[CrossRef](#)]
6. Karnaushenko, D.; Ibarlucea, B.; Lee, S.; Lin, G.; Baraban, L.; Pregel, S.; Melzer, M.; Makarov, D.; Weber, W.M.; Mikolajick, T.; et al. Light Weight and Flexible High-Performance Diagnostic Platform. *Adv. Healthc. Mater.* **2015**, *4*, 1517–1525. [[CrossRef](#)] [[PubMed](#)]
7. Ibarlucea, B.; Fawzul Akbar, T.; Kim, K.; Rim, T.; Baek, C.-K.; Ascoli, A.; Tetzlaff, R.; Baraban, L.; Cuniberti, G. Ultrasensitive detection of Ebola matrix protein in a memristor mode. *Nano Res.* **2018**, *11*, 1057–1068. [[CrossRef](#)]

8. Stern, E.; Wagner, R.; Sigworth, F.J.; Breaker, R.; Fahmy, T.M.; Reed, M.A. Importance of the Debye Screening Length on Nanowire Field Effect Transistor Sensors. *Nano Lett.* **2007**, *7*, 3405–3409. [[CrossRef](#)] [[PubMed](#)]
9. Gao, N.; Zhou, W.; Jiang, X.; Hong, G.; Fu, T.-M.; Lieber, C.M. General Strategy for Biodetection in High Ionic Strength Solutions Using Transistor-Based Nanoelectronic Sensors. *Nano Lett.* **2015**, *15*, 2143–2148. [[CrossRef](#)] [[PubMed](#)]
10. Patterson, E.I.; Prince, T.; Anderson, E.R.; Casas-Sanchez, A.; Smith, S.L.; Cansado-Utrilla, C.; Solomon, T.; Griffiths, M.J.; Acosta-Serrano, Á.; Turtle, L.; et al. Methods of Inactivation of SARS-CoV-2 for Downstream Biological Assays. *J. Infect. Dis.* **2020**, *222*, 1462–1467. [[CrossRef](#)] [[PubMed](#)]
11. Tsurkan, M.V.; Chwalek, K.; Prokoph, S.; Zieris, A.; Levental, K.R.; Freudenberg, U.; Werner, C. Defined Polymer–Peptide Conjugates to Form Cell-Instructive starPEG–Heparin Matrices In Situ. *Adv. Mater.* **2013**, *25*, 2606–2610. [[CrossRef](#)] [[PubMed](#)]

Disclaimer/Publisher’s Note: The statements, opinions and data contained in all publications are solely those of the individual author(s) and contributor(s) and not of MDPI and/or the editor(s). MDPI and/or the editor(s) disclaim responsibility for any injury to people or property resulting from any ideas, methods, instructions or products referred to in the content.